NEOPLASIA
www.neoplasia.com

Volume 16 Number 3 March 2014 pp. 235–246.e1 235

Optical Tomography of MMP Activity Allows a Sensitive Noninvasive Characterization of the Invasiveness and Angiogenesis of SCC Xenografts[1,2]

Wa'el Al Rawashdeh*, Susanne Arns*, Felix Gremse*, Josef Ehling*,†, Ruth Knüchel-Clarke†, Stefan Kray‡, Felix Spöler‡, Fabian Kiessling* and Wiltrud Lederle*

*Department of Experimental Molecular Imaging, Rheinisch-Westfaelische Technische Hochschule Aachen University, Aachen, Germany; †Institute of Pathology, University Hospital Aachen, RWTH Aachen University, Aachen, Germany; ‡Institute for Semiconductor Electronics, RWTH Aachen University, Aachen, Germany

Abstract

For improved tumor staging and therapy control, imaging biomarkers are of great interest allowing a noninvasive characterization of invasiveness. In squamous epithelial skin and cervix lesions, transition to invasive stages is associated with enhanced matrix metalloproteinase (MMP) activity, increased angiogenesis, and worsened prognosis. Thus, we investigated MMP activity as imaging biomarker of invasiveness and the potential of optical tomography in characterizing the angiogenic and invasive behavior of skin squamous cell carcinoma (SCC) xenografts. MMP activity was measured *in vivo* in HaCaT-ras A-5RT3 tumors at different angiogenic and invasive stages (onset of angiogenesis, intermediate and highly angiogenic, invasive stage) and after 1 week of sunitinib treatment by fluorescence molecular tomography–microcomputed tomography imaging using an activatable probe. Treatment response was additionally assessed morphologically by optical coherence tomography (OCT). *In vivo* MMP activity significantly differed between the groups, revealing highest levels in the highly angiogenic, invasive tumors that were confirmed by immunohistochemistry. At the onset of angiogenesis with lowest MMP activity, fibroblasts were detected in the MMP-positive areas, whereas macrophages were absent. Accumulation of both cell types occurred in both invasive groups, again to a significantly higher degree at the most invasive and angiogenic stage. Sunitinib treatment significantly reduced the MMP activity and accumulation of fibroblasts and macrophages and blocked tumor invasion that was additionally visualized by OCT. Human cervical SCCs also showed high MMP activity and a similar stromal composition as the HaCaT xenografts, whereas normal tissue was negative. This study strongly suggests MMP activity as imaging biomarker and demonstrates the high sensitivity of optical tomography in determining tumor invasiveness that can morphologically be supported by OCT.

Neoplasia (2014) 16, 235–246.e1

Abbreviations: SCC, squamous cell carcinoma; MMP, matrix metalloproteinase; ECM, extracellular matrix; FMT, fluorescence molecular tomography; μCT, micro-computed tomography; OCT, optical coherence tomography; i.d., intradermal; i.p., intraperitoneal; i.v., intravenous; s.c., subcutaneous; SMA, smooth muscle actin; VEGF, vascular endothelial growth factor; VEGFR2, vascular endothelial growth factor receptor number 2; PK, pan-keratin

Address all correspondence to: Wiltrud Lederle, Department of Experimental Molecular Imaging, Medical Faculty, Rheinisch-Westfaelische Technische Hochschule (RWTH) Aachen University, Pauwelsstr 20, 52074 Aachen, Germany. E-mail: wlederle@ukaachen.de

[1] This research was supported by the Aachen Interdisciplinary Center for Clinical Research IZKF and by the project "ForSaTum," which is cofunded by the European Union (European Regional Development Fund - Investing in your future) and the German federal state North Rhine-Westphalia (NRW). Parts of this work were funded by the Federal Ministry of Economics and Technology, Germany (grant 03EFT8NW58), cofinanced by funding of the European Social Fund (ESF).

[2] This article refers to supplementary material, which is designated by Figure W1 and is available online at www.neoplasia.com.

Received 25 September 2013; Revised 13 February 2014; Accepted 13 February 2014

http://dx.doi.org/10.1016/j.neo.2014.03.005

Introduction

In various tumor types including squamous cell carcinomas (SCCs), the invasiveness correlates with tumor progression, metastasis, and a poor clinical prognosis [1,2]. However, efficient therapy blocks tumor invasion and reduces the invasiveness [3,4]. At present, the tumor invasiveness is predominantly diagnosed on the basis of biopsies due to the lack of adequate biomarkers that can be addressed noninvasively. Hence, the noninvasive characterization of tumor invasiveness is of great interest for tumor staging and therapy control.

Tumor invasion is crucially dependent on the action of proteases such as matrix metalloproteinases (MMPs) that degrade various components of the extracellular matrix (ECM), including constituents of the basement membrane [5]. In addition to ECM degradation, MMPs can alter cell-cell adhesion, thus promoting cell motility, modulate the tumor immune response, and regulate angiogenesis and metastasis [5,6]. MMPs are secreted by tumor and stromal cells [7]. In the tumor stroma, major MMP expression that supports angiogenesis and tumor invasion has been attributed to fibroblasts and macrophages [3,8,9]. In SCCs, enhanced MMP levels and activity are observed at advanced, invasive tumor stages [3,7,8,10,11], suggesting MMP activity as valuable biomarker for tumor invasiveness.

Fluorescence molecular tomography (FMT) allows noninvasive quantitative tomographical imaging of fluorescent probes, and its high sensitivity enables the use of molecular markers. In particular, activatable probes have emerged as innovative tools for analyzing the activity of proteases like MMPs in preclinical tumor models [12,13]. Different preclinical studies have been undertaken to apply optical imaging of MMP activity for detecting early tumor stages *ex vivo* and assessing therapy effects [14–17]. However, to the best of our knowledge, near-infrared optical MMP imaging has not yet been systematically analyzed with respect to its potential in characterizing the angiogenic behavior and tumor invasiveness *in vivo*. Due to its penetration depth of at least a few millimeters, it might also be applicable for clinical tumors showing stepwise progression such as squamous epithelial skin lesions that are located superficially or squamous cervical tumors that can be reached endoscopically. Because for both tumor types the surgical procedures and therapeutic options are strongly dependent on the stage and the invasiveness of the tumors, the noninvasive characterization of tumor invasiveness by optical imaging can be of great value. In particular, that currently conclusive diagnosis is achieved by invasive biopsy that is often recurrently performed, as in the case of cervical lesions. Morphologically, tumor invasion can be detected by optical coherence tomography (OCT), a noninvasive interferometric imaging technique with growing importance in the clinical practice achieving near-microscopic resolution [18,19].

Therefore, the aim of this study was to investigate in detail MMP activity as *in vivo* biomarker of invasiveness and to assess the potential of near-infrared FMT of MMP activity in characterizing the invasiveness of HaCaT skin SCC xenografts. Because tumor invasion is crucially dependent on angiogenesis and both processes are substantially promoted by MMPs, the MMP activity was analyzed in HaCaT SCC xenografts at the onset of angiogenesis, as well as in intermediate and highly invasive and angiogenic SCCs. In addition, the effects of the angiogenesis inhibitor sunitinib on MMP activity and invasion were analyzed with respect to the potential of MMP imaging in therapy monitoring. To additionally get morphologic information of the tumor behavior, the tumor-stroma border was analyzed *ex vivo* by OCT.

Material and Methods

Tumor Inoculation

HaCaT-ras A-5RT3 SCC cells were cultured in Dulbecco's modified Eagle's medium, supplemented with 10% FBS, 1% penicillin (10000 U/ml), streptomycin (10,000 µg/ml), and 400 µg/ml geneticin G-418 sulphate (all from Gibco/Invitrogen, Carlsbad, CA USA). To obtain HaCaT-ras A-5RT3 SCC tumor xenografts that differ in invasiveness and angiogenic activity, tumors were induced by either subcutaneous (s.c.) injection of 2×10^6 HaCaT-ras A-5RT3 cells in 100 µl of culture medium or intradermal (i.d.) injection of 2×10^6 HaCaT-ras A-5RT3 cells in 30 µl of culture medium into the right flank of 6- to 8-week-old female CD-1 nude mice (Charles River, Wilmington, MA USA) [11].

As additional tumor model, 5×10^6 MLS ovarian carcinoma cells were injected s.c. in 100 µl of culture medium (minimum essential medium; 10% FBS; Gibco/Invitrogen) into the right flank of 6- to 8-week-old female CD-1 nude mice (Charles River).

Study Design and Antiangiogenic Therapy

All experiments were approved by the Governmental Review Committee on Animal Care. A total number of 26 animals were included in the studies for the HaCaT-ras A-5RT3 model. The MMP activity was analyzed in

i) early s.c. tumors at the onset of angiogenesis and invasion (n = 7), 1 week after tumor inoculation,
ii) i.d. tumors (n = 5) representing an intermediate angiogenic and invasive stage [20], 2 weeks tumor inoculation, and
iii) in s.c. advanced tumors (n = 5) of similar sizes as the i.d. tumors (average tumor size: i.d. = 67 ± 19 mm^3 i.d.; s.c. = 71 ± 22 mm^3), 2 weeks after inoculation that represent a highly angiogenic and invasive stage [6].

For the additional MLS ovarian carcinoma model, the s.c. tumors were analyzed

i) at the onset of angiogenesis and invasion (n = 4), 1 week after tumor inoculation and
ii) at the advanced stage (n = 4), 4 weeks after inoculation.

To analyze the effects of antiangiogenic therapy on the *in vivo* MMP activity, HaCaT-rasA-5RT3–bearing mice (s.c. tumors, n = 5) were treated with the clinically approved angiogenesis inhibitor sunitinib (multispecific tyrosine kinase inhibitor). Treatment was started after 1 week of tumor growth and continued for 1 week by daily intraperitoneal injection of 40 mg/kg sunitinib (Pfizer, New York City, NY USA). Untreated HaCaT-rasA-5RT3–bearing mice (s.c. tumors, n = 4) of 2 weeks were used as controls.

Activated MMPs were measured *in vivo* through FMT–micro-computed tomography (µCT) imaging using MMPSense 750 FAST (PerkinElmer, Waltham, MA USA).

After the *in vivo* measurements, the animals were killed, and the tumors were resected. For the therapy study, the tumor-stroma border was additionally assessed *ex vivo* through OCT directly after killing. *In vivo* and *ex vivo* data were validated by immunohistochemical analyses.

Clinical Samples

Frozen samples of invasive cervical SCC and adjacent healthy cervical tissue were generously provided by the Department of Pathology at University Hospital of Aachen (Aachen, Germany) in accordance with the ethics committee.

Fluorescence Molecular Tomography

For assessing the MMP activity *in vivo*, MMPSense 750 FAST (PerkinElmer) targeting a broad range of MMPs including MMP-2, MMP-3, MMP-7, MMP-9, MMP-12, and MMP-13 was injected i.v. into the mice through a tail vein catheter (2 nmol, total volume of 100 µl per injection). MMP activity was measured 6 hours after probe injection using an *in vivo* fluorescence tomograph (FMT 2500; PerkinElmer) [21]. The mice were anesthetized with isoflurane during imaging and fixed at a definite position in a dual-modality animal bed (CT Imaging GmbH, Erlangen, Germany).

Microcomputed Tomography and Data Reconstruction

For organ and accurate signal localization, µCT was performed directly before the FMT scan using a dual-energy µCT system (Tomoscope Duo CT; CT Imaging GmbH). The mice were kept anesthetized and fixed in the same animal bed for both µCT and FMT. The following scan protocol was used: Both tubes were run at 65 kV and 0.38 mA. Each flat panel detector acquired 720 projections in the binned mode at 25 frames per second, containing 516 × 506 pixels with a pixel size of 100 µm. A full rotation with a total scan time of 29 seconds was performed, and two subscans were acquired, each covering 3 cm in the axial direction. After scanning, a Feldkamp-type reconstruction was performed at isotropic voxel size of $(70\ \mu m)^3$ using a ring artifact reduction method and a soft reconstruction kernel.

Quantitative three-dimensional FMT data and volumetric µCT data were fused using automated detection of markers as described in Kunjachan et al [22]. MMPSense 750 FAST concentrations in the tumors were determined using Amide's a Medical Imaging Data Examiner (AMIDE) after having set regions of interest on the basis of the anatomic µCT data [23,24].

Optical Coherence Tomography

Excised s.c tumors were scanned *ex vivo* in a dual-band OCT system centered at 830 nm and 1220 nm. 2-dimensional (2D) OCT images were taken from various planes within each tumor. The skin covering the tumors was peeled off before scanning due to the high scattering of the horn layer and to account for the restricted imaging depth of the OCT (~ 1.5 mm). Clinically relevant OCT bandwidths were chosen with 830 nm providing higher resolution (as used in ophthalmology) and 1220 nm offering a higher penetration depth (as used endoscopically) [18,25,26].

In situ Zymography and Indirect Immunofluorescence

Tumors were excised, scanned with OCT, afterwards deep frozen at – 80°C, and cut into 8-µm slices. The MMP activity was detected *in situ* using a gelatinase assay (EnzCheck Gelatinase/Collagenase Assay Kit; Invitrogen). Unfixed tumor sections were incubated with the DQ substrate (Invitrogen, Carlsbad, CA USA) (40 µg/ml) for 30 minutes. After washing (3 × 10 minutes), the sections were fixed, and subsequent immunofluorescence staining was performed as described previously [27]. The following primary antibodies were applied: a biotinylated antibody against smooth muscle actin (SMA) (α-SMA biotin; Progen Pharmaceuticals [PROGEN Biotechnik GmbH, Heidelberg, Germany]) to depict cancer-associated fibroblasts, an antibody targeting F4/80-positive macrophages (anti-mouse F4/80 rat; AbD Serotec, Kidlington, UK), a CD31-specific antibody (anti-mouse CD31 rat; BD Biosciences, San Jose, CA USA) for staining the endothelium, an antibody against vascular endothelial growth factor receptor 2 (VEGFR2) (anti-mouse VEGFR2 goat; R&D Systems, Minneapolis, MN USA) for analyzing the angiogenic activity, and an antibody against keratins [anti-human pan keratin (PK) guinea pig; Progen Pharmaceuticals] for staining the tumor cells. Corresponding secondary antibodies were used as previously described [27]. Cell nuclei were counterstained by 49,6-diamidino-2-phenylindole (DAPI; Invitrogen).

For human samples, anti-human CD31 (anti-human CD31 rabbit; Acris Antibodies GmBH, Herford, Germany), anti-VEGFR2 (anti-human VEGFR2 mouse, Dianova, Hamburg, Herford, Germany), and anti-CD68 (anti-human CD68 rat, against macrophages, AbD Serotec, Kidlington, UK) antibodies were used. Staining was done as described [27].

Stained sections were examined and photographed with the Carl Zeiss Axio Imager M2 (Carl Zeiss, Jena, Germany). Images were quantified by determining the percentage of immunofluorescent positive area fractions. For each tumor, four to seven micrographs including the top, bottom, both sides, and the center were analyzed using the AxioVision Rel 4.8 software (Carl Zeiss).

Statistics

A two-tailed Student's *t* test was applied for statistical analysis using Excel (Microsoft, Redmond, WA USA). A *P* value of less than .05 was considered as statistically significant, a *P* value of less than .01 as highly significant, and a *P* value of less than .001 as very highly significant.

Results

MMP Activity as Imaging Biomarker of the Angiogenic Status and Invasiveness of HaCaT SCC Xenografts

Because enhanced MMP expression and activity are associated with angiogenesis, tumor progression, and invasion in different tumor types including SCCs, we investigated MMP activity as biomarker of invasiveness and the potential of *in vivo* MMP imaging in the noninvasive characterization of tumor invasiveness and the angiogenic activity. We used the HaCaT-ras A-5RT3 SCC model because it had been well characterized in a previous study [11] for the *in vivo* expression of MMP-2, MMP-3, MMP-9, and MMP-13 that are targeted by the near-infrared probe MMPSense 750 FAST. Enhanced expression and activity of these MMPs have been observed in various tumors including SCCs [6,10]. The MMP activity was therefore measured *in vivo* by FMT-µCT imaging and compared in HaCaT-ras A-5RT3 SCC xenografts at different stages of angiogenesis and invasiveness, in s.c. tumors at the onset of angiogenesis and invasion, in i.d. tumors representing an intermediate angiogenic and invasive stage, and in s.c. advanced, highly angiogenic, and invasive tumors (Figure 1, *A*–*C*).

The *in vivo* MMP activity significantly differed between the groups. Highest levels were measured in the advanced, highly angiogenic, and invasive s.c. HaCaT-ras A-5RT3 tumors, followed by the i.d. tumors at the intermediate stage, whereas lowest activity was recorded for s.c. tumors at the onset of angiogenesis and invasion (Figure 2, *A* and *C*). This was confirmed *ex vivo* on tumor sections by *in situ* zymography (Figure 2, *B* and *D*).

In the tumor microenvironment, fibroblasts and macrophages have been identified as strong MMP-expressing cells that promote angiogenesis and tumor invasion [3]. We therefore analyzed the presence of SMA-positive fibroblasts and F4/80-positive macrophages in the HaCaT-ras A-5RT3 tumors at differential angiogenic and

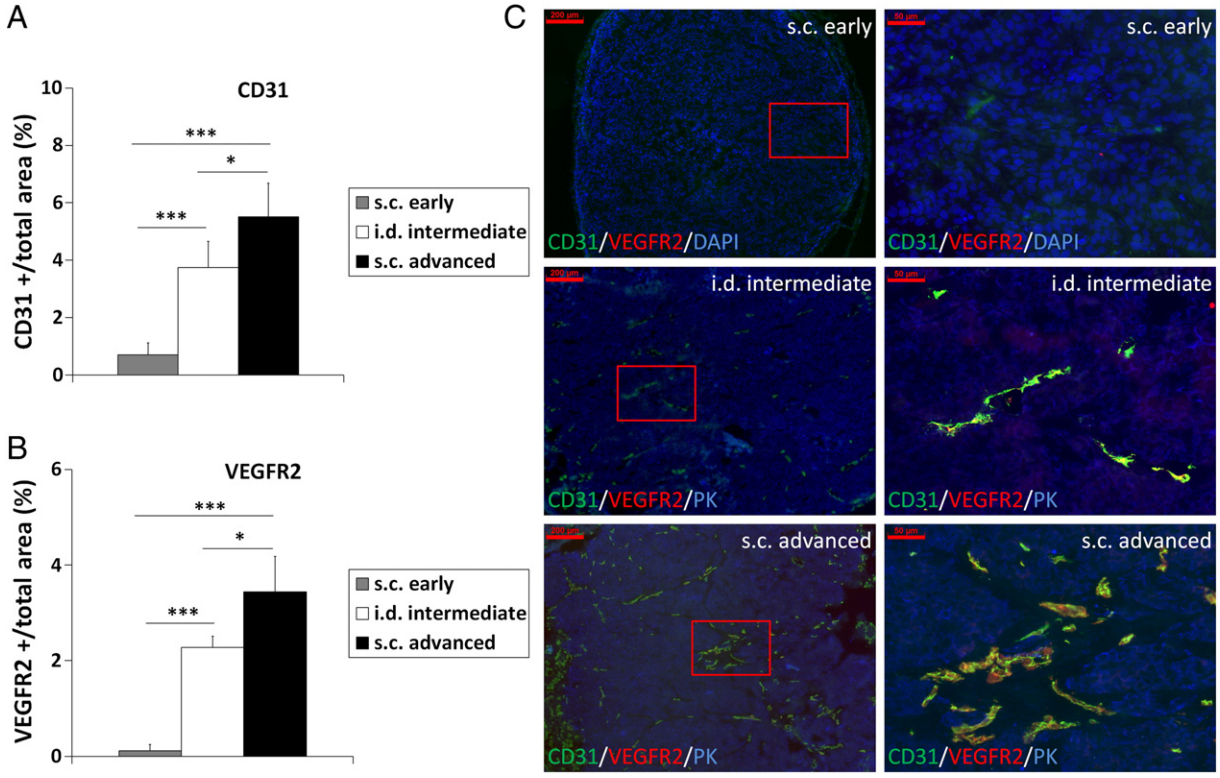

Figure 1. HaCaT-ras A-5RT3 variants represent different angiogenic and invasive stages. Quantification (A and B) of immunostainings for CD31 and VEGFR2 (C) shows the highest vessel density (A and C), angiogenic activity (B and C), and invasiveness (C) in s.c. advanced tumors ($n = 5$), whereas i.d. tumors ($n = 5$) have an intermediate angiogenic and invasive stage, and s.c. early tumors are at the onset of angiogenesis and invasion ($n = 7$). (C) Representative immunostainings of the different HaCaT-ras A-5RT3 variants for CD31 (green), VEGFR2 (red), DAPI (blue), or PK (blue), respectively. Right panels (bar, 50 μm) are magnified selected areas of the left panels (bar, 200 μm) (indicated by the red square). Data are presented as means ± SD (*$P < .05$ and ***$P < .001$).

invasive stages. Both, the SMA- and F4/80-positive area fractions were significantly higher in advanced s.c. than in i.d. ($P < .01$ for both) and early s.c. tumors ($P < .001$ for both), demonstrating the strongest presence of fibroblasts and macrophages in the tumors with highest angiogenic activity and strongest invasiveness (Figure 3, *A* and *B*; representative immunostainings are shown in Figure 3*C*). Interestingly, whereas SMA-positive fibroblasts were observed in early s.c. tumors at the onset of angiogenesis, even in vessel-free areas, no macrophages were detected at this stage.

To expand the application and to further analyze the sensitivity of *in vivo* MMP imaging in determining the invasiveness and angiogenic activity of tumors, MMP activity was additionally measured *in vivo* in s.c. ovarian carcinoma xenografts (MLS) at an early (1 week post-injection) and advanced stages (4 weeks post-injection) by FMT-μCT imaging. Comparably to the HaCaT-ras A-5RT3 tumors, MMP activity *in vivo* and *ex vivo* also significantly differed between the differential stages in the MLS tumors, confirming the sensitivity of *in vivo* MMP imaging and the suitability of MMP activity as imaging biomarker of invasiveness and angiogenesis (Figure W1).

Optical Tomography of MMP activity Accurately Depicts the Reduced Angiogenesis and Invasion After Antiangiogenic Treatment with Sunitinib

MMPs are crucially involved in angiogenesis, and MMP activity has been shown to correlate with the degree of angiogenesis and tumor invasion in the HaCaT-ras A-5RT3 xenografts. Previous work on differentially aggressive HaCaT xenografts had demonstrated that VEGFR2 blockade by DC101 strongly reduced MMP expression and activity and resulted in reversion to a premalignant noninvasive tumor phenotype [28,29]. We therefore investigated the effects of the strong angiogenesis inhibitor sunitinib on angiogenesis and invasion and whether MMP imaging could also depict the effects of the therapy on tumor angiogenesis and invasion. To this end, tumor-bearing mice were treated for 1 week with sunitinib after 1 week of tumor growth, and the MMP activity was compared with 2-week-old highly angiogenic and invasive untreated controls.

Sunitinib treatment resulted in a significantly lower microvessel density and angiogenic activity compared with untreated controls (Figure 4, *A* and *B*, representative immunostainings are shown in Figure 4*C*; $P < .001$ for both). In addition, tumor invasion was inhibited in the sunitinib-treated mice, where the tumors appeared encapsulated with regular borders and necrotic areas in the center (Figures 4*C* and 5*D*).

Optical tomography revealed a significantly lower *in vivo* MMP activity in sunitinib-treated mice compared with the untreated controls (Figure 5*A*; $P < 0.001$; representative images shown in Figure 5*C*). In agreement with the *in vivo* data, a significantly decreased MMP activity was detected *ex vivo* on the sections of the treated tumors compared with the controls (Figure 5*B*; $P < .01$; representative immunostainings are shown in Figure 5*D*).

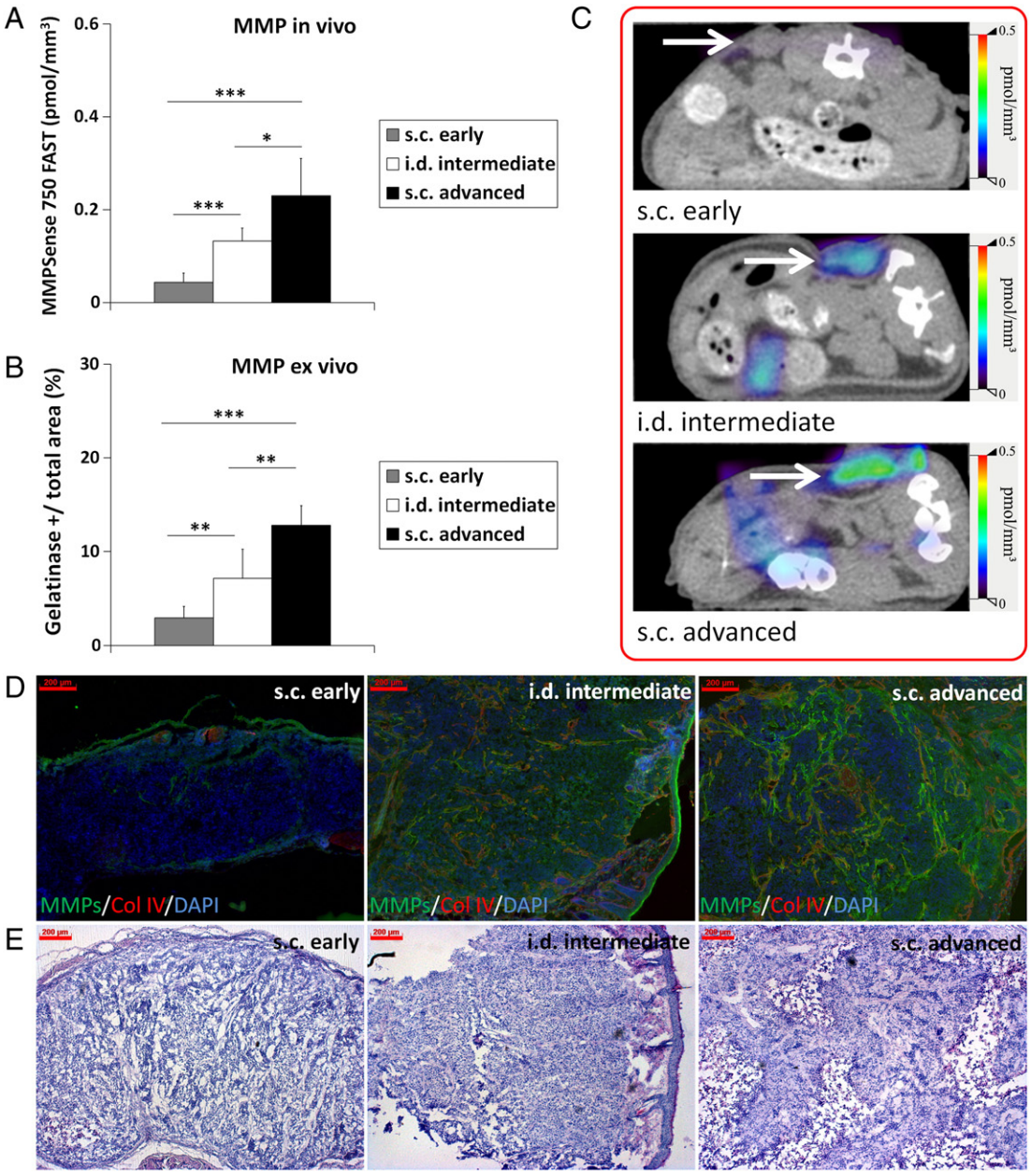

Figure 2. MMP activity differs significantly between the HaCaT-A-5RT3 tumors at differential angiogenic and invasive stages. (A) Assessment of MMP activity *in vivo* by FMT-μCT imaging reveals significant differences in intratumoral concentrations of activated MMPSense 750 FAST between s.c. advanced ($n = 5$), i.d. intermediate ($n = 5$), and s.c. early ($n = 7$) tumors. Highest concentrations are recorded for s.c. advanced tumors at the highly angiogenic and invasive stage, whereas lowest concentrations are found in s.c. early tumors at the onset of angiogenesis and invasion. (B) Quantification of *in situ* zymography of MMP activity on tumor sections confirms the *in vivo* data. (C) Representative FMT/μCT fusion images of tumor-bearing mice (transverse plane) show the fluorescent signals of activated MMPSense 750 FAST in s.c. early, i.d., and s.c. advanced tumors (tumors indicated by a white arrow). The additional fluorescent signals found in the intestine region can occur from hepatobiliary excretion of the probe through the intestine. (D) Representative images of *in situ* zymography of MMP activity (green) [counterstained with collagen IV (red) and DAPI (blue)] of an s.c. early-stage tumor at the onset of angiogenesis and invasion, an i.d. tumor at the intermediate angiogenic and invasion stage, and an s.c. advanced, highly angiogenic, and invasive tumor. (E) Representative H&E staining of the different HaCaT-ras A-5RT3 tumors. Bar, 200 μm. Data are presented as means ± SD (*$P < .05$, ** $P < .01$, and ***$P < .001$).

When further analyzing the accumulation of fibroblasts and macrophages, the amount of both cell types was significantly reduced in the sunitinib-treated tumors compared with the untreated controls, as shown by the significantly lower SMA- and F4/80-positive area fractions, respectively (Figure 6, *A* and *B*; $P < .001$ for fibroblasts and $P < .01$ for macrophages; representative immunostainings are shown in Figure 6*C*).

OCT Depicts Reduced Tumor Invasion After Sunitinib Treatment

To further characterize the tumor invasion at a morphologic level, the tumors were scanned *ex vivo* using a dual-band OCT system. An irregular tumor border zone was detected in the untreated 2-week-old s.c. HaCaT-ras A-5RT3 tumors (Figure 7*A*). In contrast, the sunitinib-treated tumors were clearly separated from the upper

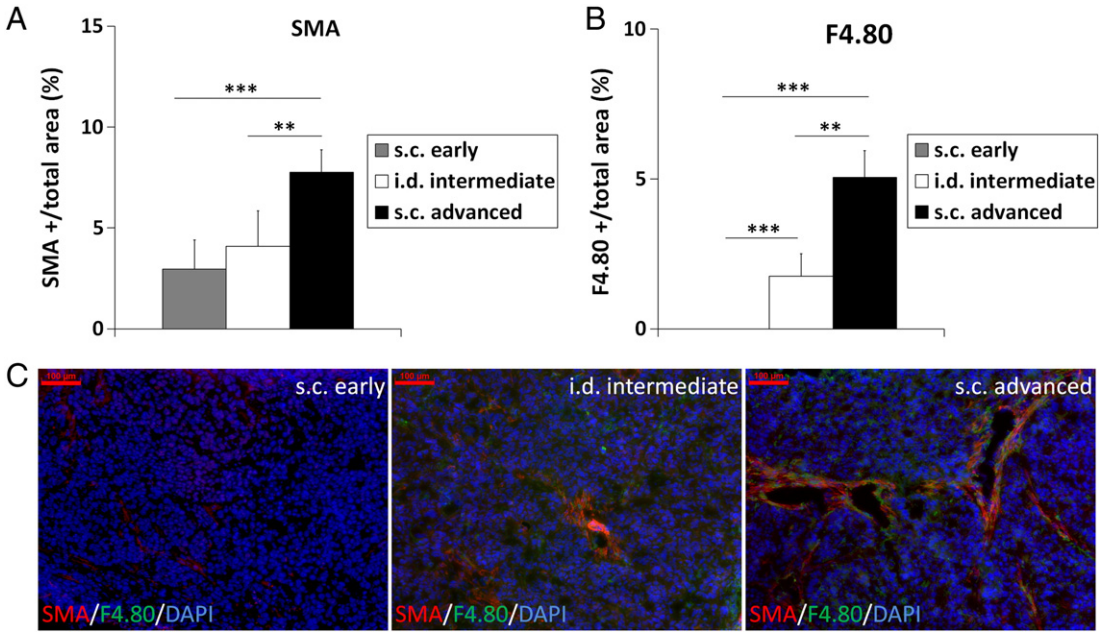

Figure 3. Quantification of SMA-positive fibroblasts (A) and F4/80-positive macrophages (B) shows a differential accumulation at the distinct stages of angiogenesis and invasion. Highest accumulation of these cells is found in s.c. advanced tumors at the highest angiogenic and invasive stage. Notably, no macrophages are detected in the s.c. early tumors at the onset of angiogenesis and invasion. (C) Representative immunostainings for SMA (red), F4/80 (green), and DAPI (blue) of an s.c. early tumor at the onset of angiogenesis, an i.d. tumor at intermediate stage of angiogenesis and invasion, and an s.c. advanced, highly angiogenic, and invasive tumor. Bar, 100 μm. Data are presented as means ± SD (**$P < .01$ and ***$P < .001$; s.c. early: $n = 7$, i.d. intermediate: $n = 5$, and s.c. advanced: $n = 5$).

dermis by a regular line, indicating reduced invasion and normalization of the tumor border zone (Figure 7*B*). Immunohistochemical analysis of the corresponding tumor sections confirmed the irregular tumor border in the untreated tumors with invasive, infiltrating tumor protrusions (Figure 7*C*), whereas invasion was blocked by sunitinib treatment, and the border of the encapsulated tumors was well demarcated and partially collagen IV positive (Figure 7*D*). These data demonstrate that OCT allows the morphologic characterization of the tumor behavior at a high resolution (Figure 7).

MMP Activity and Stromal Composition of Clinical SCCs are Similar to the HaCaT SCC Xenografts

To analyze whether MMP activity is also a biomarker of invasiveness in clinical SCCs, we analyzed the MMP activity in invasive cervical SCC

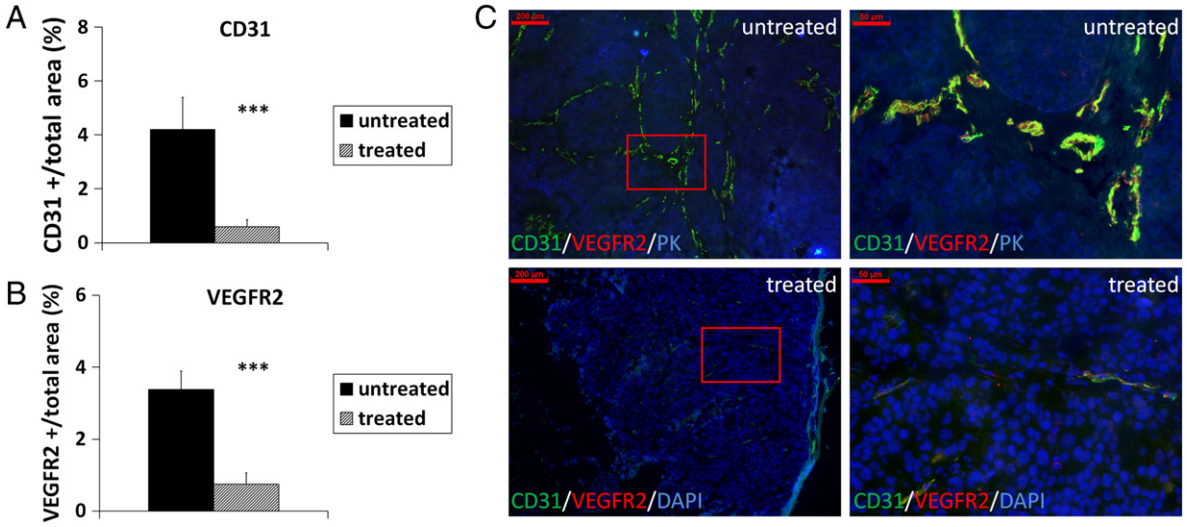

Figure 4. Sunitinib treatment results in strong reduction of angiogenesis and blocks invasion of s.c. HaCaT-ras A-5RT3 tumors. Quantification of immunostainings for CD31 and VEGFR2 demonstrates the significant reduction in vessel density (A) and angiogenic activity (B) in sunitinib-treated tumors ($n = 5$) compared with untreated controls ($n = 4$). (C) Representative immunostainings for CD31 (green), VEGFR2 (red), keratin (PK; blue), or DAPI (blue), respectively, of an untreated control and sunitinib-treated tumor. Right panels (bar, 50 μm) are magnified selected areas of the left panels (bar, 200 μm) (indicted by a red square). Data are presented as means ± SD. (***$P < .001$).

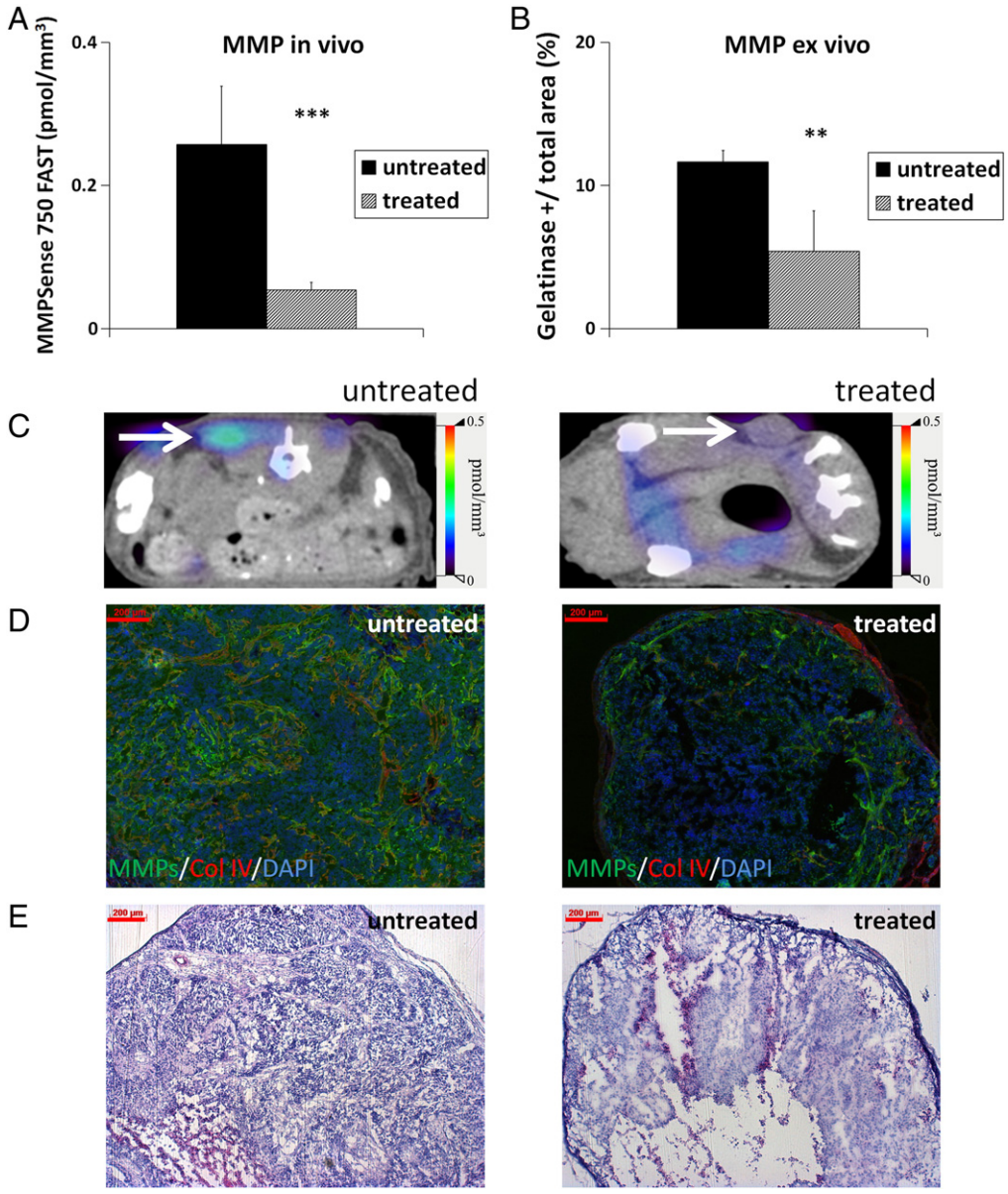

Figure 5. Sunitinib treatment significantly reduces MMP activity in HaCaT-rasA-5RT3 tumors. (A) Assessment of MMP activity *in vivo* by FMT/μCT hybrid imaging demonstrates significantly decreased concentrations of activated MMPSense 750 FAST in sunitinib-treated tumors (***$P <$ .001; $n = 5$) compared with untreated controls ($n = 4$). (B) Quantification of *in situ* zymography of MMP activity on tumor sections confirms again the *in vivo* results. (C) Representative FMT/μCT fusion images of tumor-bearing mice (transverse plane) show the fluorescent signals of activated MMPSense 750 FAST in an untreated control and sunitinib-treated tumor (tumors indicated by a white arrow). (D) Representative images of *in situ* zymography of MMP activity (green) counterstained with collagen IV (red) and DAPI (blue) of an untreated control and sunitinib-treated tumor. (E) Representative H&E staining of the different HaCaT-ras A-5RT3 tumors. Bar, 200 μm. Data are presented as means ± SD (**$P <$ .01 and ***$P <$ .001).

biopsies and adjacent normal cervical tissue by *in situ* zymography. Whereas no MMP activity was found in normal cervical tissue, a strong MMP activity was detected in stromal strands of cervical SCC samples, showing similarities to the advanced s.c. highly invasive HaCaT-ras A-5RT3 tumors (Figure 8, *A* and *B*). Strong eosin-positive, collagen-enriched strands were detected in the invasive tumor areas of the SCCs, whereas no ECM-enriched areas were found in normal cervical samples by hematoxylin and eosin (H&E) staining (Figure 8, *C* and *D*). Moreover, a strong infiltration of SMA-positive fibroblasts and macrophages was detected in the cervical SCCs, whereas SMA-positive fibroblasts were absent in the normal cervical tissue, and the amount of macrophages was markedly lower (Figure 8, *E* and *F*). This confirmed the strong up-regulation of MMP activity in invasive cervical human SCCs compared with healthy cervical tissue (Figure 8*A*) and a similar stromal composition as in the HaCaT-ras A-5RT3 SCC xenografts.

Discussion

In tumors that develop stepwise such as SCCs of the skin and the cervix, the invasiveness correlates with tumor progression, metastasis, and a worse clinical prognosis and is predominantly diagnosed by invasive biopsies [1–4]. In addition, surgical and therapeutic strategies in these tumors depend on the tumor stage. Hence, distinct imaging biomarkers that allow a noninvasive characterization of tumor invasion are of great interest for improving tumor

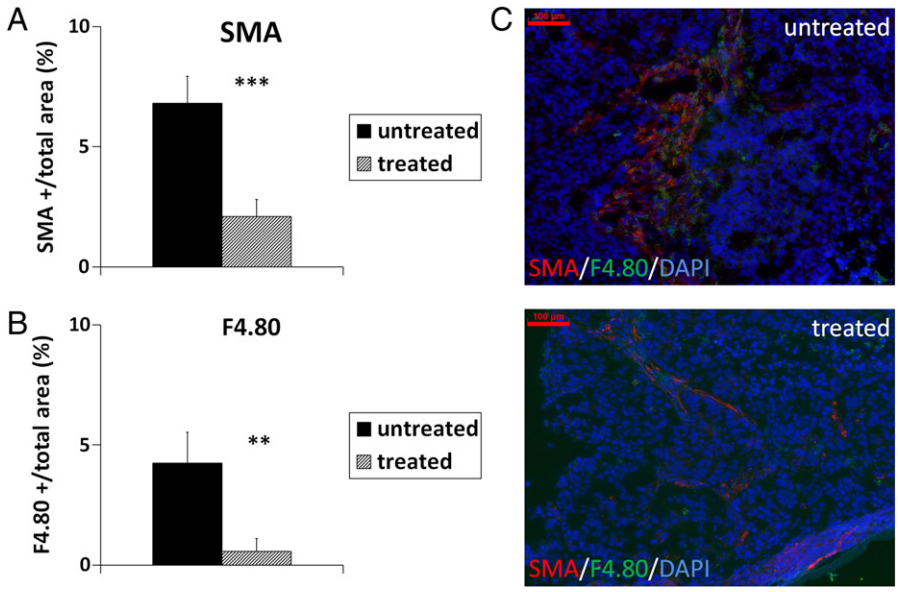

Figure 6. Quantification of SMA-positive fibroblasts (A) and F4/80-positive macrophages (B) shows the significantly reduced accumulation of both cell types in sunitinib-treated s.c. HaCaT-rasA-5RT3 tumors compared with the untreated controls. (C) Representative immunostainings for SMA (red), F4/80 (green), and DAPI (blue) of an untreated control and a sunitinib-treated tumor. Bar, 100 μm. Data are presented as means ± SD (**$P < .01$ and ***$P < .001$; untreated controls: $n = 4$; sunitinib-treated tumors: $n = 5$).

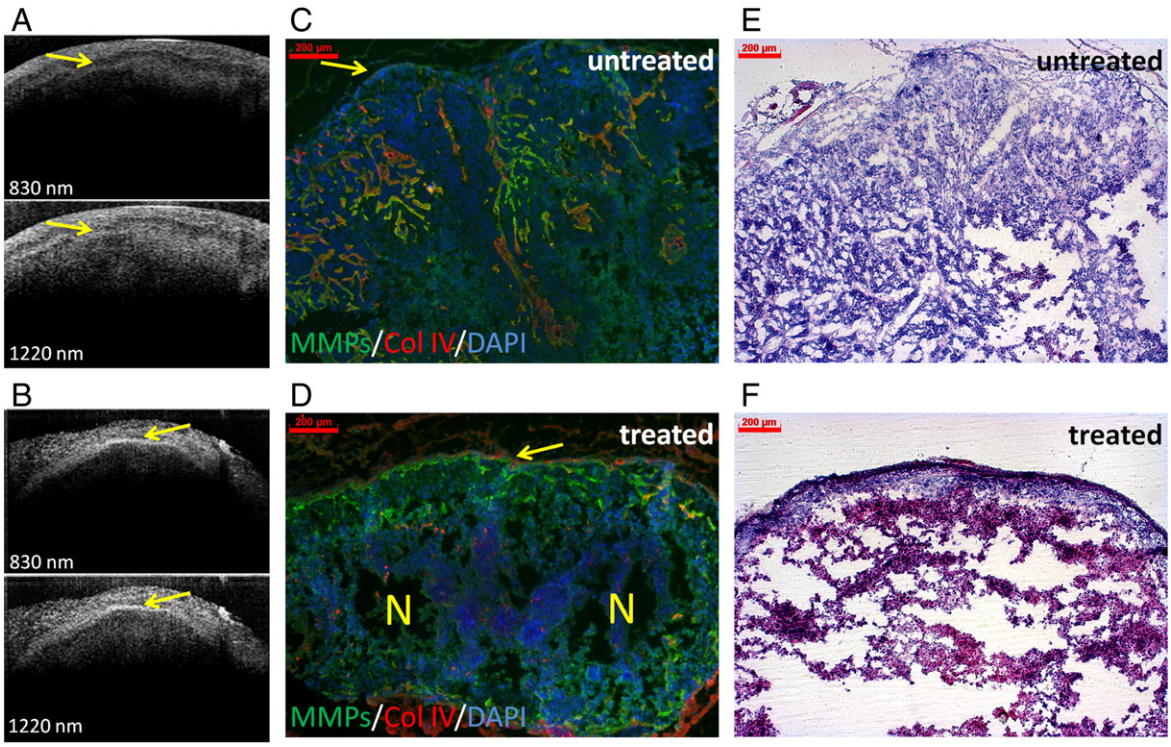

Figure 7. OCT depicts the blockade of invasion after sunitinib treatment at the morphologic level. Morphologic characterization of the tumor border by dual-band OCT clearly shows the blockade of invasion after treatment of HaCaT-rasA-5RT3–bearing mice with sunitinib. OCT images (800 and 1220 nm, respectively) of an untreated control (A) and a sunitinib-treated tumor (B). Note the irregular tumor border (indicated by a yellow arrow), typical characteristics of invasion of the untreated control (A), whereas the tumor is separated from the upper dermis by a regular line in the sunitinib-treated tumor (B, indicated by a yellow arrow). (C and D) *In situ* zymography of MMP activity and counterstaining for collagen IV (red) and DAPI (blue) on corresponding tumor sections demonstrate the irregular tumor border with invasive, infiltrating tumor cell protrusions (indicated by a yellow arrow) in the untreated control tumor (C). In contrast, tumor invasion is blocked after sunitinib treatment, and the tumor is encapsulated and well demarcated from the stroma (D). Note also the partial deposition of collagen IV deposition at the border (indicated by a yellow arrow) and the necrotic area in the center (indicated by a yellow N). (E and F) Representative H&E staining of the different HaCaT-ras A-5RT3 tumors. OCT image size: 2.5 * 1.6 mm. Bar, 200 μm.

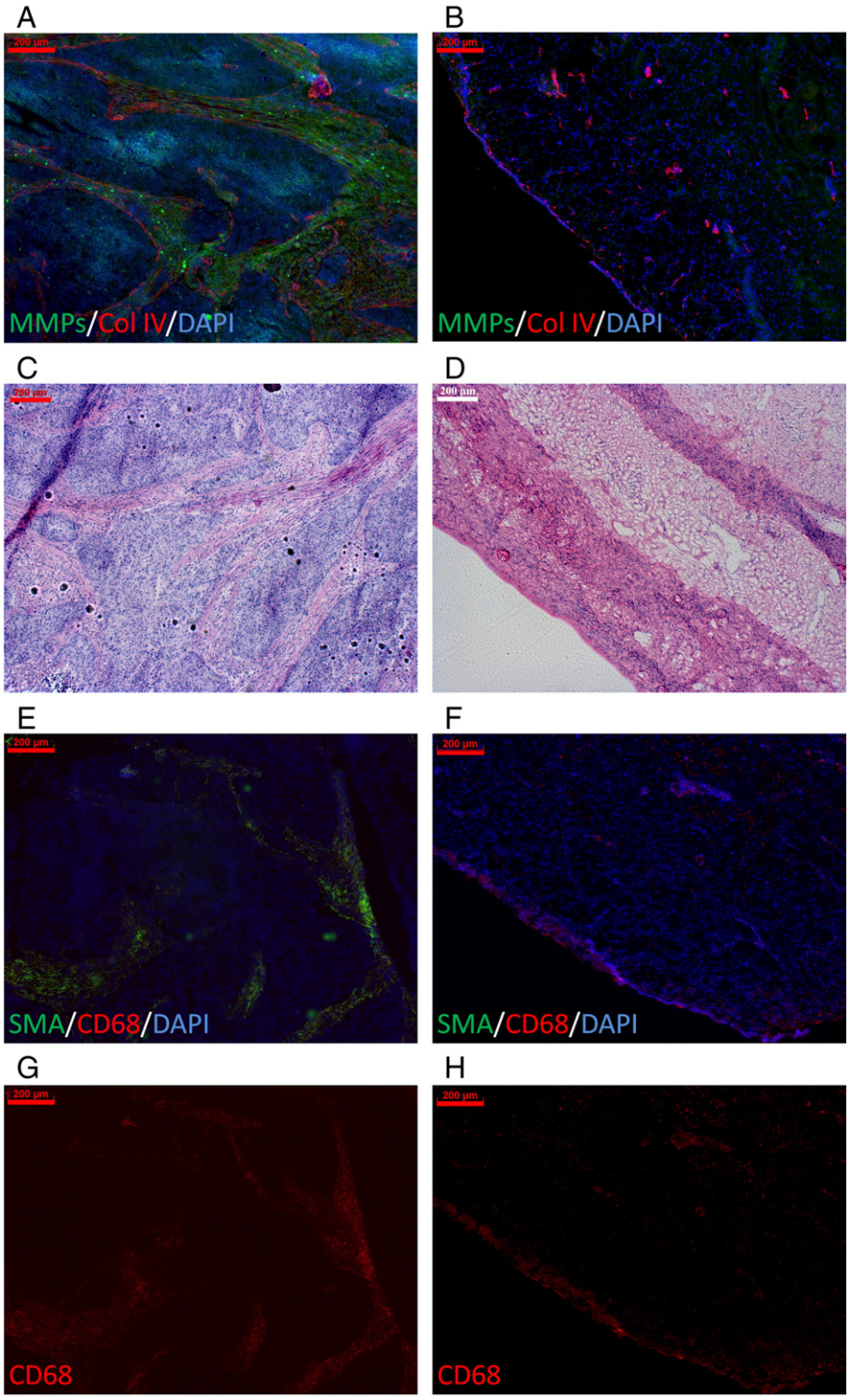

Figure 8. Human cervical SCC samples show also a high MMP activity and a similar stroma composition as the HaCaT-SCC xenografts. *In situ* zymography of MMP activity (green) and counterstaining for collagen IV (red) and DAPI (blue) of human samples reveals the strong MMP activity in the invasive cervical SCC (A), whereas the healthy tissue is negative (B). H&E staining demonstrates strong eosin-positive, collagen-enriched stromal strands in the cervical SCC (C) that resemble the strands seen in the s.c. advanced highly invasive HaCaT-ras A-5RT3 tumors, whereas in the healthy cervical tissue (D), no ECM-enriched areas are obvious. (E–G) Immunostaining for SMA-positive fibroblasts and CD68-positive macrophages shows the strong infiltration of these cell types in the cervical SSC (E and G), whereas SMA-positive fibroblasts are absent in healthy cervical tissue, and markedly fewer macrophages are detected (F and H). SMA (green), CD68 (red), and DAPI (blue). Bar, 200 μm.

staging and therapy control. In this regard, MMPs have been identified as key players in promoting tumor cell invasion and dissemination, and enhanced activity is usually found at invasive, advanced tumor stages and associated with a poor clinical prognosis [1,2,30,31]. In addition, MMPs regulate angiogenesis, a crucial process promoting sustained tumor growth, dissemination, and metastasis [32,33]. However, MMPs are downregulated in response to cancer therapies, including efficient antiangiogenic therapy [8,29].

This suggests that the MMP activity might be a promising imaging biomarker for noninvasive tumor staging and therapy control. In this context, optical imaging of MMP activity using biocompatible near-infrared fluorogenic MMP substrates as activatable reporter probes has been established for about a decade as innovative technique and allows a sensitive detection of MMP activity *in vivo* [14,34,35]. Moreover, hybrid imaging allows unambiguous association of fluorescent signal to the respective organs, increasing the reproducibility of the analysis [22].

Thus, the aim of our study was to investigate MMP activity as an *in vivo* biomarker of tumor invasiveness and angiogenesis and to assess the potential of noninvasive optical tomography of MMP activity in characterizing skin SCC xenografts that differ in invasiveness and angiogenic activity. In addition, MMP imaging was assessed with respect to monitoring of antiangiogenic therapy by sunitinib. Analysis was done in the HaCaT-ras A-5RT3 model that had been well characterized in a previous study [11] with regard to *in vivo* expression of MMP-2, MMP-3, MMP-9, and MMP-13 that are targeted by the probe MMPSense 750 FAST.

To this end, the MMP activity was measured *in vivo* in early s.c. HaCaT-ras A-5RT3 tumors at the onset of angiogenesis and invasion (1 week post-injection) in advanced highly invasive and angiogenic s. c. tumors (around 2 weeks post-injection) and in i.d. injected HaCaT-ras A-5RT3 tumors (around 2 weeks post-injection) of a similar size as the advanced s.c. tumors representing an intermediate invasive and angiogenic stage. Optical tomography of MMP activity sensitively discriminated between the xenografts at different invasive and angiogenic stages, revealing significant differences in the activity between all groups. Highest *in vivo* activity was measured in the advanced, highly angiogenic, and invasive s.c. HaCaT-ras A-5RT3 tumors, whereas lowest activity was recorded for the early s.c. tumors at the onset of angiogenesis. This was confirmed *ex vivo* on tumor sections by *in situ* zymography, demonstrating the high accuracy of *in vivo* MMP imaging. The results strongly suggest that MMP activity is a useful imaging marker of SCC invasiveness. Previous studies performed by other groups have already demonstrated that near-infrared imaging of MMP activity has a high sensitivity and accuracy in detecting early colon tumor stages *ex vivo* [16,17]. However, we here provide evidence of the high sensitivity and accuracy of near-infrared optical tomography for discriminating differential stages of tumor angiogenesis and invasiveness in living mice *in vivo*. Additional analysis of a s.c. ovarian carcinoma xenograft model at differential stages of angiogenesis and invasiveness also revealed significant differences in the *in vivo* MMP activity comparably to the HaCaT-ras A-5RT3 xenografts, thus confirming the sensitivity of *in vivo* MMP imaging and the suitability of MMP activity as imaging biomarker of invasiveness and angiogenesis.

Further immunohistochemical analyses of the tumor sections revealed the strongest accumulation of SMA-positive fibroblasts and F4/80-positive macrophages in s.c. advanced, highly angiogenic, and invasive tumors, being also significantly higher than in i.d. tumors at the intermediate stage. Both fibroblasts and macrophages have been demonstrated to promote angiogenesis, tumor invasion, and progression by secreting cytokines (e.g., VEGF), chemokines, and MMPs [7,8]. Thus, the significantly enhanced accumulation of these cell types can explain the highest MMP activity as well as the strongest angiogenesis and invasiveness of the advanced s.c. tumors. Interestingly, no macrophages were detected in early s.c. tumors at the onset of angiogenesis and invasion, whereas SMA-positive fibroblasts were present within the intratumoral stromal strands, even in vessel-free areas. These findings are in line with our previous studies on skin SCCs showing that fibroblasts crucially promote angiogenesis by expression of cytokines and MMPs like MMP-13 [7,27]. The delayed infiltration of macrophages at stages with enhanced vascularization suggests that they are predominantly recruited through the bloodstream, probably also triggered by cytokine induction in fibroblasts [3]. This further suggests that initial growth and invasion of these tumors are promoted by fibroblasts, whereas inflammation additionally maintains angiogenesis and invasion at advanced stages [36].

Previous studies in differentially aggressive HaCaT SCC xenografts had revealed that antiangiogenic therapy with DC101 revert the tumor phenotype to a premalignant noninvasive stage, accompanied by a strong reduction in MMP expression and activity [28,29]. We therefore investigated the MMP activity as *in vivo* biomarker for therapy control and whether MMP imaging can depict the effects of antiangiogenic therapy on tumor invasion. Sunitinib, a clinically used US Food and Drug Administration (FDA)-approved multispecific tyrosine kinase inhibitor, was used due to its known strong antiangiogenic effects [37].

As expected, treatment of HaCaT-rasA-5RT3–bearing mice for 1 week with sunitinib resulted in a significantly reduced angiogenesis and microvessel density compared with the untreated controls. In addition, antiangiogenic therapy blocked tumor invasion, resulting in encapsulated tumors with necrotic areas in the center that were well demarcated from the stroma and at the border partially positive for the basement membrane component collagen IV. In line with the reduced invasiveness, optical tomography demonstrated a significantly lower MMP activity in the sunitinib-treated tumor-bearing mice *in vivo*, being again confirmed *ex vivo*. Further immunohistochemical analyses revealed a significantly lower accumulation of fibroblasts and macrophages after sunitinib treatment. Although antiangiogenic therapy has previously been shown to almost abrogate the infiltration of SMA-positive fibroblasts in tumor-bearing mice [29], we believe that reduced macrophage accumulation occurred as a consequence of blood vessel regression, thus impairing the recruitment of monocytes from the blood circulation. This demonstrates that antiangiogenic therapy efficiently reduced the MMP activity, "normalized" the stroma, and inhibited tumor invasion. Furthermore, MMP activity has been shown as a suitable imaging biomarker for monitoring inhibition of tumor invasion in response to efficient antiangiogenic therapy.

To further analyze the effects of antiangiogenic therapy at the morphologic level, the excised tumors were analyzed *ex vivo* by dual-band OCT. The OCT system covers two clinically relevant bandwidths centered at 830 nm and 1220 nm, providing higher image resolution at 830 nm and a higher penetration depth at 1220 nm, respectively [18,25,26]. Whereas an irregular tumor border zone was detected in the untreated s.c. HaCaT-ras A-5RT3 tumors, typical morphologic characteristics of invasive tumors, the tumor was clearly demarcated from the mouse stroma by a regular precise line after sunitinib treatment. Immunohistochemical analyses of corresponding tumor sections confirmed the irregular tumor stroma border in the untreated controls with invasive, infiltrating tumor areas and the regular borders of the encapsulated tumor after sunitinib treatment. These data further highlight the potential of OCT in the noninvasive morphologic characterization of tumors at high resolution.

To analyze whether enhanced MMP activity was also an indicator of tumor invasiveness in clinical SCCs, cervical SCC and adjacent healthy cervix tissues were analyzed by *in situ* zymography. A high MMP activity was detected within stromal strands in the invasive areas of the cervical cancer samples, closely resembling those found in advanced s.c. HaCaT-ras A-5RT3 tumors. In contrast, no MMP activity was detected in healthy cervical tissue. In addition, a pronounced stromal infiltrate of SMA-positive fibroblasts and macrophages was found in invasive cervical carcinomas, closely resembling the stromal composition of the HaCaT xenografts.

These findings support the hypothesis that MMP activity is a useful imaging marker of SCC invasiveness. Because skin and cervical carcinoma development involves typical progression stages (dysplasia, carcinoma *in situ*, and invasive carcinoma) and MMP up-regulation is associated with transition to the invasive stage [2,38-40], our results suggest that near-infrared imaging of MMP activity might have potential in the noninvasive staging of squamous skin lesions that are located superficially or cervical lesions that can be reached endoscopically. A more profound noninvasive characterization of these lesions by molecular MMP imaging additionally to white light illumination for detection might be of great value because both the surgical and therapeutic interventions in these tumor entities strongly depend on the tumor stage [41,42]. However, whether MMP imaging might be feasible in the clinic for initial detection of lesions needs further investigation. A first *in vivo* endoscopic approach of detecting active proteases by near-infrared imaging with potential for clinical translation has been undertaken by Alencar et al. [43]. They used a modified near-infrared imaging microcatheter, combining white light and fluorescence, with a protease-activatable probe, cathepsin B, that allowed a sensitive early detection of colon tumors in mice *in vivo*, which might potentially decrease the miss rate of neoplastic colon lesions and increase the speed of colonic examinations [43].

In light of the recent developments, the results of the study further suggest that a combination of near-infrared optical imaging and OCT might be beneficial for obtaining noninvasive information of both MMP activity and morphologic characteristics to improve staging or therapy control of cancers such as cervical or skin SCCs. Future applications of combined imaging are suggested as optical biopsies for superficial skin tumors or endoscopic/ laparoscopic applications in cervical lesions, including guidance and assistance in intraoperative surgery.

References

[1] Habbous S, Pang V, Eng L, Xu W, Kurtz G, Liu FF, Mackay H, Amir E, and Liu G (2012). p53 Arg72Pro polymorphism, HPV status and initiation, progression, and development of cervical cancer: a systematic review and meta-analysis. *Clin Cancer Res* **18**, 6407–6415.

[2] Boukamp P (2005). Non-melanoma skin cancer: what drives tumor development and progression? *Carcinogenesis* **26**, 1657–1667.

[3] Allen M and Jones JL (2011). Jekyll and Hyde: the role of the microenvironment on the progression of cancer. *J Pathol* **233**, 162–176.

[4] Mueller MM and Fusenig NE (2004). Friends or foes – bipolar effects of the tumour stroma in cancer. *Nat Rev Cancer* **4**, 839–849.

[5] McCawley LJ and Matrisian LM (2001). Tumor progression: defining the soil round the tumor seed. *Curr Biol* **11**, R25-27.

[6] Shuman Moss LA, Jensen-Taubman S, and Steller-Stevenson WG (2012). Matrix metalloproteinases: Changing roles in tumor progression and metastasis. *Am J Pathol* **181**, 1895–1899.

[7] Lederle W, Hartenstein B, Meides A, Kunzelmann H, Werb Z, Angel P, and Mueller MM (2010). MMP13 as a stromal mediator in controlling persistent angiogenesis in skin carcinoma. *Carcinogenesis* **31**, 1175–1184.

[8] Li H, Fan X, and Houghton JM (2007). Tumor microenvironment: the role of the tumor stroma in cancer. *J Cell Biochem* **101**, 805–815.

[9] Mantovoni A, Biswas SK, Galdiero MR, Sica A, and Locati M (2013). Macrophages plasticity and polarization in tissue repair and remodeling. *J Pathol* **229**, 176–185.

[10] Egeblad M and Werb Z (2002). New functions for the matrix metalloproteinases in cancer progression. *Nat Rev Cancer* **2**, 161–174.

[11] Vosseler S, Lederle W, Airola K, Obermueller E, Fusenig NE, and Mueller MM (2009). Distinct progression-associated expression of tumor and stromal MMPs in HaCaT skin SCCs correlates with onset of invasion. *Int J Cancer* **125**, 2296–2306.

[12] Ntziachristos V, Ripoll J, Wang LV, and Weissleder R (2005). Looking and listening to light: the evolution of whole-body photonic imaging. *Nat Biotechnol* **23**, 313–320.

[13] Ntziachristos V, Bremer C, and Weissleder R (2003). Fluorescence imaging with near-infrared light: new technological advances that enable *in vivo* molecualr imaging. *Eur Radiol* **13**, 195–208.

[14] Bremer C, Bredow S, Mahmood U, Weissleder R, and Tung CH (2001). Optical imaging of matrix metalloproteinase-2 activity in tumors: Feasibility study in a mouse model. *Radiology* **221**, 523–529.

[15] Hensley HH, Roder NA, O'Brien SW, Bickel LE, Xiao F, Litwin S, and Connolly DC (2012). Combined *in vivo* molecular and anatomic imaging for detection of ovarian carcinoma-associated protease activity and integrin expression in mice. *Neoplasia* **14**, 451–462.

[16] Yoon SM, Myung SJ, Ye BD, Kim IW, Lee NG, Ryu YM, Park K, Kim K, Kwon IC, and Park YS, et al (2010). Near-infrared fluorescence imaging using a protease-specific probe for the detection of colon tumors. *Gut Liver* **4**, 488–497.

[17] Clapper ML, Hensley HH, Chang WC, Devarajan K, Nguyen MT, and Cooper HS (2011). Detection of colorectal adenomas using a bioactivatable probe specific for matrix metalloproteinases activity. *Neoplasia* **13**, 685–691.

[18] Hermes B, Spöler F, Naami A, Bornemann J, Först M, Grosse J, Jakse G, and Knüchel R (2008). Visualization of the basement membrane zone of the bladder by optical coherence tomography: Feasibility of noninvasive evaluation of tumor invasion. *Urology* **72**, 676–681.

[19] Al Rawashdeh W, Kray S, Pich A, Pargen S, Balaceanu A, Lenz M, Spöler F, Kiessling F, and Lederle W (2012). Polymeric nanoparticles as OCT contrast agents. *J Nanoparticle Res* **14**, 1255. http://dx.doi.org/10.1007/s11051-012-1255-0.

[20] Bonnotte B, Gough M, Phan V, Ahmen A, Chong H, Martin F, and Vile RG (2003). Intradermal injection, as opposed to subcutaneous injection, enhances immunogenicity and suppresses tumorigenicity of tumor cells. *Cancer Res* **63**, 2145–2149.

[21] Montet X, Ntziachristos V, Grimm J, and Weissleder R (2005). Tomographic fluorescence mapping of tumor targets. *Cancer Res* **65**, 6330–6336.

[22] Kunjachan S, Gremse F, Theek B, Koczera P, Pola R, Pechar M, Etrych T, Ulbrich K, Storm G, and Kiessling F, et al (2013). Noninvasive optical imaging of nanomedicine biodistribution. *ACS Nano* **7**, 252–262. http://dx.doi.org/10.1021/nn303955n#_blank.

[23] Loening AM and Gambhir SS (2003). AMIDE: a free software tool for multimodality medical image analysis. *Mol Imaging* **2**, 131–137.

[24] Gremse F and Schulz V (2011). In: Kiessling F, Pichler BJ, editors. Small Animal Imaging: *Qualitative and quantitative data analysis*. Berlin Heidelberg: Springer; 2011. p. 363–378.

[25] Kray S, Spöler F, and Kurz H (2009). Improved contrast in clinical imaging. *SPIE Newsroom*. http://dx.doi.org/10.1117/2.1200909.1809.

[26] Welzel J (2001). Optical coherence tomography in dermatology: a review. *Skin Res Technol* **7**, 1–9.

[27] Lederle W, Linde N, Heusel J, Bzyl J, Woenne EC, Zwich S, Skobe M, Kiessling F, Fusenig NE, and Mueller MM (2010). Platelet-derived growth factor-B normalizes micromorphology and vessel function in vascular endothelial growth factor- A-induced squamous cell carcinomas. *Am J Pathol* **176**, 981–994.

[28] Skobe M, Rockwell P, Goldstein N, Vosseler S, and Fusenig NE (1997). Halting angiogenesis suppresses carcinoma cell invasion. *Nat Med* **3**, 1222–1227.

[29] Vosseler S, Mirancea N, Bohlen P, Mueller MM, and Fusenig NE (2005). Angiogenesis inhibition by vascular endothelial growth factor receptor-2 blockage reduces stromal matrix metalloproteinase expression, normalizes stromal tissue, and reverts epithelial tumor phenotype in surface heterotransplants. *Cancer Res* **65**, 1294–1305.

[30] Kanayama H (2010). Matrix metalloproteinases and bladder cancer. *J Med Invest* **48**, 31–43.
[31] Hartenstein B, Dittrich BT, Stickens D, Heyer B, Vu TH, Teurich S, Schorpp-Kistner M, Werb Z, and Angel P (2006). Epidermal development and wound healing in matrix metalloproteinase 13-deficient mice. *J Invest Dermatol* **126**, 486–496.
[32] Lu Z, Jiang G, Blume-Jensen P, and Hunter T (2011). Epidermal growth factor-induced tumor cell invasion and metastasis initiated by dephosphorylation and downregulation of focal adhesion kinase. *Mol Cell Biol* **21**, 4016–4031.
[33] Yokota J (2000). Tumor progression and metastasis. *Carcinogenesis* **21**, 497–503.
[34] Bremer C, Tung CH, and Weissleder R (2001). *In vivo* molecular target assessment of matrix metalloproteinase inhibition. *Nat Med* **7**, 743–748.
[35] Bremer C, Ntziachristos V, and Weissleder R (2003). Optical-based molecualr imaging: cotrast agents and potential medical applications. *Eur Radiol* **13**, 231–243.
[36] Linde N, Lederle W, Depner S, van Rooijen N, Gutschalk CM, and Mueller MM (2012). Vascular endothelial growth factor-induced skin carcinogenesis depends on recruitment and alternative activation of macrophages. *J Pathol* **227**, 17–28.
[37] Rix A, Lederle W, Siepmann M, Fokong S, Behrendt FF, Bzyl J, Grouls C, Kiessling F, and Palmowski M (2012). Evaluation of high frequency ultrasound methods and contrast agents for characterizing tumor response to anti-angiogenic treatment. *Eur J Radiol* **81**, 2710–2716.
[38] Kumar V, Abbas AK, Fausto N, and Mitchell RN (2007). Robbins Basic Pathology. 8th ed. Saunders Elsevier. ISBN 978-1-4160-2973-1; 2007. p. 718–721.
[39] Walboomers JM, Jacobs MV, Manos MM, Bosch FX, Kummer JA, Shah KV, Snijders PJ, Peto J, Meijer CJ, and Muñoz N (1999). Human papillomavirus is a necessary cause of invasive cervical cancer worldwide. *J Pathol* **189**, 12–19.
[40] Campbell S and Monga A (2006). Gynaecology by Ten Teachers. 18th ed. UK: Hodder Education. ISBN 0-340-81662-7; 2006.
[41] Motley R, Kersey P, and Lawrence C, British Association of Dermatologists, British Association of Plastic Surgeons, Royal College of Radiologists, Faculty of Clinical Oncology (2002). Multiprofessional guidelines for the management of the patient with primary cutaneous squamous cell carcinoma. *Br. J. Dermatol* **146**, 18–25.
[42] Beckmann MW (2004.). S2-Leitlinien Diagnostik und Therapie des Zervixkarzinoms. Darmstadt: Zuckschwerdt Verlag; 2004.
[43] Alencar H, Funovics MA, Figueiredo J, Sawaya H, Weissleder R, and Mahmood U (2007). Colonic adenocarcinoma: near-infrared microcatheter imaging of smart probes for early detection—study in mice. *Radiology* **244**, 232–238.

Supplementary Materials

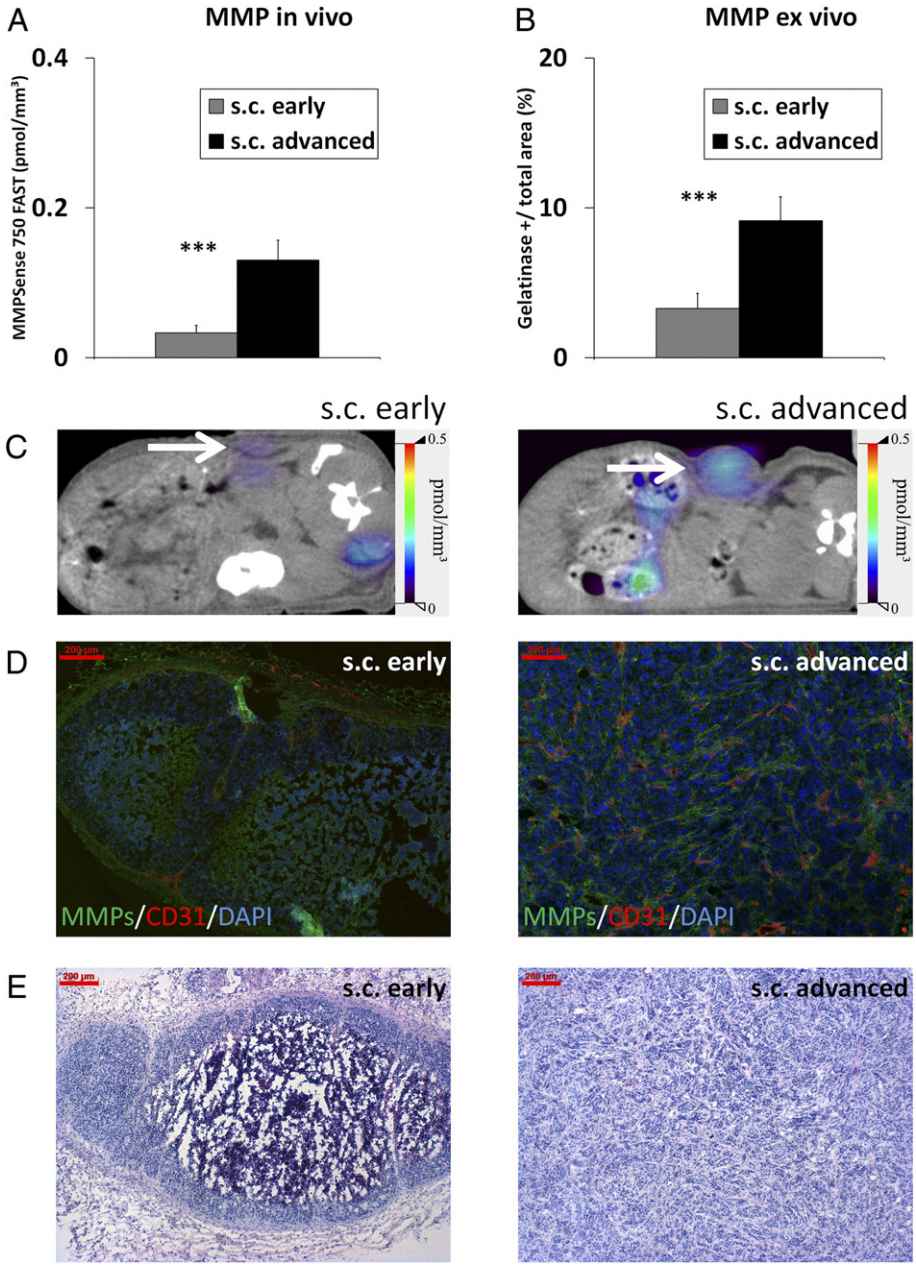

Figure W1. MMP activity differs significantly between MLS tumors at differential invasive and angiogenic stages. (A) Assessment of MMP activity *in vivo* by FMT-μCT imaging reveals significantly higher concentrations of activated MMPSense 750 FAST in s.c. advanced ($n = 4$) compared with s.c. early ($n = 4$) MLS tumors. (B) Quantification of *in situ* zymography of MMP activity on tumor sections confirms the *in vivo* data. (C) Representative FMT/μCT fusion images of tumor-bearing mice (transverse plane) show the fluorescent signals of activated MMPSense 750 FAST in s.c. early and s.c. advanced tumors (tumors indicated by a white arrow). (D) Representative images of *in situ* zymography of MMP activity (green) counterstained with CD31 (red) and DAPI (blue) of an s.c. early and an s.c. advanced MLS tumor. (E) Representative H&E staining of the different MLS tumors. Bar, 200 μm. Data are presented as means ± SD (***$P < .001$).